MOLECULAR BIOLOGY

The nuclear transcription factor, TAF7, is a cytoplasmic regulator of protein synthesis

Dan Cheng[1], Kevin Semmens[2], Elizabeth McManus[1], Qingrong Chen[3], Daoud Meerzaman[3], Xiantao Wang[4], Markus Hafner[4], Brian A. Lewis[5], Hidehisa Takahashi[6], Ballachanda N. Devaiah[1], Anne Gegonne[1], Dinah S. Singer[1]*

The TFIID component, TAF7, has been extensively characterized as essential for transcription and is critical for cell proliferation and differentiation. Here, we report that TAF7 is a previously unknown RNA chaperone that contributes to the regulation of protein synthesis. Mechanistically, TAF7 binds RNAs in the nucleus and delivers them to cytoplasmic polysomes. A broad spectrum of target RNA species, including the HIV-1 transactivation response element, binds TAF7 through consensus CUG motifs within the 3′ untranslated region. Export to the cytoplasm depends on a TAF7 nuclear export signal and occurs by an exportin 1–dependent pathway. Notably, disrupting either TAF7's RNA binding or its export from the nucleus results in retention of target messenger RNAs in the nucleus and reduced levels of the protein products of TAF7-target RNAs. Thus, TAF7, an essential transcription factor, plays a key role in the regulation of RNA translation, thereby potentially connecting these processes.

INTRODUCTION

Transcription and translation in eukaryotic cells are each tightly regulated processes with multiple steps that ensure appropriate levels of synthesis. These two processes need to be coordinately regulated to maintain cellular homeostasis. While coordination between transcription and translation is well established in prokaryotes, less is known about the integration of eukaryotic transcription and translation. In yeast, the RNA polymerase II heterodimer Rpb4/7 cotranscriptionally binds its target RNAs and regulates their cytoplasmic stability (*1*, *2*). The splicing factor SRSF1 has been reported to indirectly regulate transcription, RNA export, and translation in mammalian cells (*3*). The nuclear transcription factor p53 has been shown to have a cytoplasmic function that regulates translation primarily through its interaction with components of the translation machinery (*4*). However, there is no evidence to date that these pleiotropic activities function to directly coordinate transcription and translation. Here, we have explored the possibility that the transcription factor TATA box–binding protein (TBP)–associated factor 7 (TAF7) provides such coordination.

The transcription factor TAF7 plays a critical role in regulating many of the steps in transcription. As a component of the general transcription factor complex, TFIID, TAF7 interacts with the TAF1 component and inhibits its acetyltransferase activity, which is essential for transcription initiation (*5*–*7*). TAF7 is released from TAF1 once the assembly of the transcription preinitiation complex is complete, allowing transcription to initiate (*8*). TAF7 also binds to and inhibits the kinase activity of each of the polymerase II (Pol II) C-terminal repeat domain (CTD) kinases involved in initiation, pause release, and elongation—namely, TFIIH, bromodomain containing 4 (BRD4), and positive transcription elongation factor b (P-TEFb), respectively. It then travels with the transcription elongation machinery into the gene body (*9*, *10*). Thus, TAF7 serves as a critical checkpoint regulator that prevents these transcription factors from functioning prematurely, ensuring that each step of transcription is completed before proceeding to the next step (*8*, *11*).

The requirement for TAF7 in transcription varies among different cell types. In general, the requirement for TAF7 is greater in proliferating cells than in quiescent, differentiated cells. Depletion of TAF7 in both human embryonic kidney–293T and mouse embryonic cells inhibits transcription of genes regulating proliferation (*12*). Similarly, deletion of TAF7 in vivo in immature mouse thymocytes inhibits transcription globally, resulting in the abrogation of their proliferation and differentiation. In contrast, TAF7 deletion affects only a small number of transcripts in resting peripheral CD4 T cells (*13*).

Although most studies have focused on the transcriptional functions of TAF7, there is some evidence to suggest that the role of TAF7 extends beyond transcription regulation. TAF7 has been shown to associate with the 160-kDa subunit of cleavage-polyadenylation specificity factor, which is required for 3′ polyadenylation of mRNA (*14*). In *Schizosaccharomyces pombe*, mutations in Ptr6p, a homolog of human TAF7, results in the accumulation of RNA in the nucleus (*15*).

Considering our previous findings that TAF7 travels with Pol II and the nascent transcript during elongation, we hypothesized that TAF7 associates with RNA and executes functions beyond transcriptional regulation. We have now found that TAF7 is an RNA-binding protein that recognizes the consensus motif CUG in the 3′ untranslated region (3′UTR) and associates with a large spectrum of RNA species. TAF7 chaperones its target RNAs from the nucleus to polysomes in the cytoplasm, where it contributes to the regulation of translation. Disruption of TAF7 binding to RNA or depletion of cytoplasmic TAF7 results in a global reduction in protein synthesis and a specific reduction in the levels of protein products of its target RNAs. We propose a model in which regulation of transcription and translation are linked through a mechanism in which the transcription factor TAF7 delivers target RNAs from the nucleus to cytoplasmic polysomes, thereby regulating translation.

[1]Experimental Immunology Branch, National Cancer Institute, NIH, Bethesda, MD 20892, USA. [2]School of Medicine, University of Utah, Salt Lake City, UT 84132, USA. [3]Center for Biomedical Informatics and Information Technology, National Cancer Institute, NIH, Rockville, MD 20850, USA. [4]Laboratory of Muscle Stem Cells and Gene Regulation, National Institute of Arthritis and Musculoskeletal and Skin Diseases, NIH, Bethesda, MD 20892, USA. [5]Laboratory of Pathology, National Cancer Institute, NIH, Bethesda, MD 20892, USA. [6]Department of Molecular Biology, Yokohama City University Graduate School of Medical Science, Fukuura 3-9, Kanazawa-ku, Yokohama, Kanagawa 216-0004, Japan.
*Corresponding author. Email: dinah.singer@nih.gov

RESULTS

TAF7 localizes in both the nucleus and cytoplasm

As a component of the general transcription factor TFIID and a regulator of transcription, TAF7 is only known to function in the nucleus. Therefore, it was unexpected to observe substantial levels of TAF7 in the cytoplasm of HeLa cells by immunofluorescence with anti-TAF7 antibodies (Fig. 1A and fig. S1A). Cellular fractionation of both HeLa and mouse B lymphoma cells further demonstrated the presence of a remarkable concentration of cytoplasmic TAF7 (Fig. 1B and fig. S1B). The enrichment of TAF7 in the cytoplasm was quantified relative to the nuclear TAF7 and to the total cellular TAF7. Since nuclear TAF7 is associated with TFIID, and its integral component TBP, the relative enrichment of TAF7 in the cytoplasm was compared with the relative amount of TBP, which is nuclear and corrected for cytoplasmic tubulin (Fig. 1B and fig. S1, B and C). Cytoplasmic TAF7 represents nearly one-half of the total TAF7 in the cell (Fig. 1C). This cytoplasmic localization is not true of other TAFs. For example, in HeLa cells, neither TAF6 nor TAF12 is detected in the cytoplasm above the level of TBP (fig. S1, C and D). Therefore, in addition to its association with the TFIID complex in the nucleus, the transcription factor TAF7 occurs at substantial levels in the cytoplasm independent of other TFIID components.

Cytoplasmic TAF7 is associated with polysomes

The existence of significant levels of cytoplasmic TAF7 led us to ask whether TAF7 exists as an independent factor in the cytoplasm or in a complex as it does with TFIID in the nucleus. Cytoplasmic extracts of HeLa cells were subjected to fast protein liquid chromatography (FPLC) column fractionation, and the elution profile of TAF7 was assessed by immunoblotting. Unexpectedly, cytoplasmic TAF7, a protein of 55 kDa, eluted at a position equivalent to 440 kDa, indicating that it is associated with a multiprotein complex; no TBP was detected in this complex (Fig. 1D and fig. S1E). In contrast, nuclear TAF7 coeluted with TFIID at a size greater than 1 MDa (fig. S1F). In a parallel analysis of cytoplasmic extracts from the TMD8 B lymphoma cell line, TAF7 also eluted in a 440-kDa complex (fig. S1E). Cytoplasmic TAF7 occurs in a complex completely distinct from that of TFIID.

To characterize the composition of the large TAF7-containing cytoplasmic complex, an anti-TAF7 immunoprecipitate from HeLa cell extracts was analyzed by mass spectrometry. Ribosomal proteins, primarily 60S proteins, were the most abundant peptides identified (fig. S1G). Among the ribosomal proteins identified, the large ribosomal subunit proteins, RPL5 and RPL8, were chosen for further validation of their association with TAF7. Proximity ligation assay (PLA) of HeLa cells documented that TAF7 colocalizes with both RPL5 and RPL8 in situ with the associations largely restricted to the cytoplasm (Fig. 1, E and F, and fig. S1H). In contrast, no significant colocalization of TBP was observed with either RPL5 or RPL8 (Fig. 1, E and F). Furthermore, in anti-FLAG immunoprecipitates of cytoplasmic extracts from HeLa cells stably transfected with FLAG-tagged TAF7 {HeLa TAF7 [wild type (WT)]}, both RPL5 and RPL8 were detected (fig. S1I). Direct immunoprecipitation (IP) of TAF7 with two different anti-TAF7 antibodies also coimmunoprecipitated RPL5 and RPL8, confirming the association (fig. S1J).

The finding of colocalization of TAF7 with ribosomal proteins in situ suggested that cytoplasmic TAF7 is associated with polysomes. To assess this possibility, cytoplasmic extracts of HeLa TAF7 (WT) cells were fractionated in a sucrose gradient. The sedimentation profile of monosomes and polysomes was determined by OD_{254}, and the distribution of TAF7 was analyzed by immunoblotting of each fraction. TAF7 cosedimented with RPL5 in both polysome and monosome fractions (Fig. 1G). Together, these results demonstrate that TAF7 is associated with ribosomal proteins and polysomes.

TAF7 binds RNAs in vitro and in vivo

The association of TAF7 with polysomes could be either through direct binding to ribosomal proteins or indirectly through RNA. To distinguish these possibilities, we first tested whether TAF7 binds RNA either in vitro or in vivo. Recombinant TAF7 protein or a control protein, bovine serum albumin (BSA), was incubated with total RNA extracted from HeLa cells, followed by IP with an anti-TAF7 antibody to isolate TAF7-RNA complexes; RNA in the complexes was 3′ end–labeled, extracted, and run on an RNA gel. As shown in Fig. 1H, TAF7 immunoprecipitated a broad spectrum of RNA species. Thus, TAF7 binds to RNA in vitro.

To determine whether TAF7 also binds RNA in cells, whole cell extracts from HeLa TAF7 (WT) cells were immunoprecipitated with anti-TAF7 antibody. Immunoprecipitated RNA was extracted, 3′ end–labeled, and examined on an RNA gel. As shown in Fig. 1I, anti-TAF7, but not control mouse immunoglobulin G (IgG), coimmunoprecipitated a spectrum of RNA species from HeLa cells. Furthermore, IP with anti-FLAG of extracts from HeLa cells stably transfected with TAF7 or with a truncation mutant deleted of the TAF7 C-terminal segment 130 to 349 amino acids, TAF7 (1 to 129), or with a vector control, revealed that TAF7 coimmunoprecipitated a broad spectrum of RNAs (Fig. 1J). In contrast to full-length TAF7, TAF7 (1 to 129) did not coimmunoprecipitate RNA (Fig. 1J), mapping the RNA binding domain (RBD) to the C-terminal two-thirds of the molecule. Thus, TAF7 binds to multiple RNA species, both in vitro and in vivo, identifying it as an RNA binding protein.

TAF7 contains an RBD and nuclear localization and export signals

Since the TAF7 truncation mutant, TAF7 (1 to 129), was unable to bind RNA (Fig. 1J), an RBD maps between 130 and 349 amino acids. To further map the RBD, a series of mutants were generated (Fig. 2A). In in vitro RNA binding assays, we found that deletion of a segment spanning amino acids 131 to 163 was unable to bind RNA (Fig. 2B, and fig. S2, A and B). To fine-map the RBD, amino acid substitutions were made in the segments 134 to 142 and 140 to 155. Mutation of amino acids between 140 and 155 [TAF7 (RBD)], but not between 134 and 142, abrogated binding to RNA, mapping the TAF7 RBD within this segment (Fig. 2B and fig. S2A). The RNA binding site of TAF7 is highly homologous to that of HIV-1 Tat (fig. S2C).

The translocation of proteins over 40 kDa into or out of the nucleus is generally dependent on active transport mediated by nuclear localization signals (NLS) and nuclear export signals (NES) (*16*). Since TAF7 is a 55-kDa protein, we reasoned that TAF7 would have an NLS to mediate its nuclear localization. The TAF7 (1 to 129) truncation mutant is entirely cytoplasmic, whereas a TAF7 (1 to 202) mutant localizes to the nucleus, suggesting the presence of an NLS between amino acids 129 and 202 (fig. S2, D and E). Analysis of the TAF7 amino acid sequence revealed a potential NLS that overlaps the TAF7 RBD in the central region of the molecule between amino acids 140 and 155 (Fig. 2A) [cNLS Mapper (http://nls-mapper.iab.keio.ac.jp/cgi-bin/NLS_Mapper_form.cgi)]. Therefore, we examined

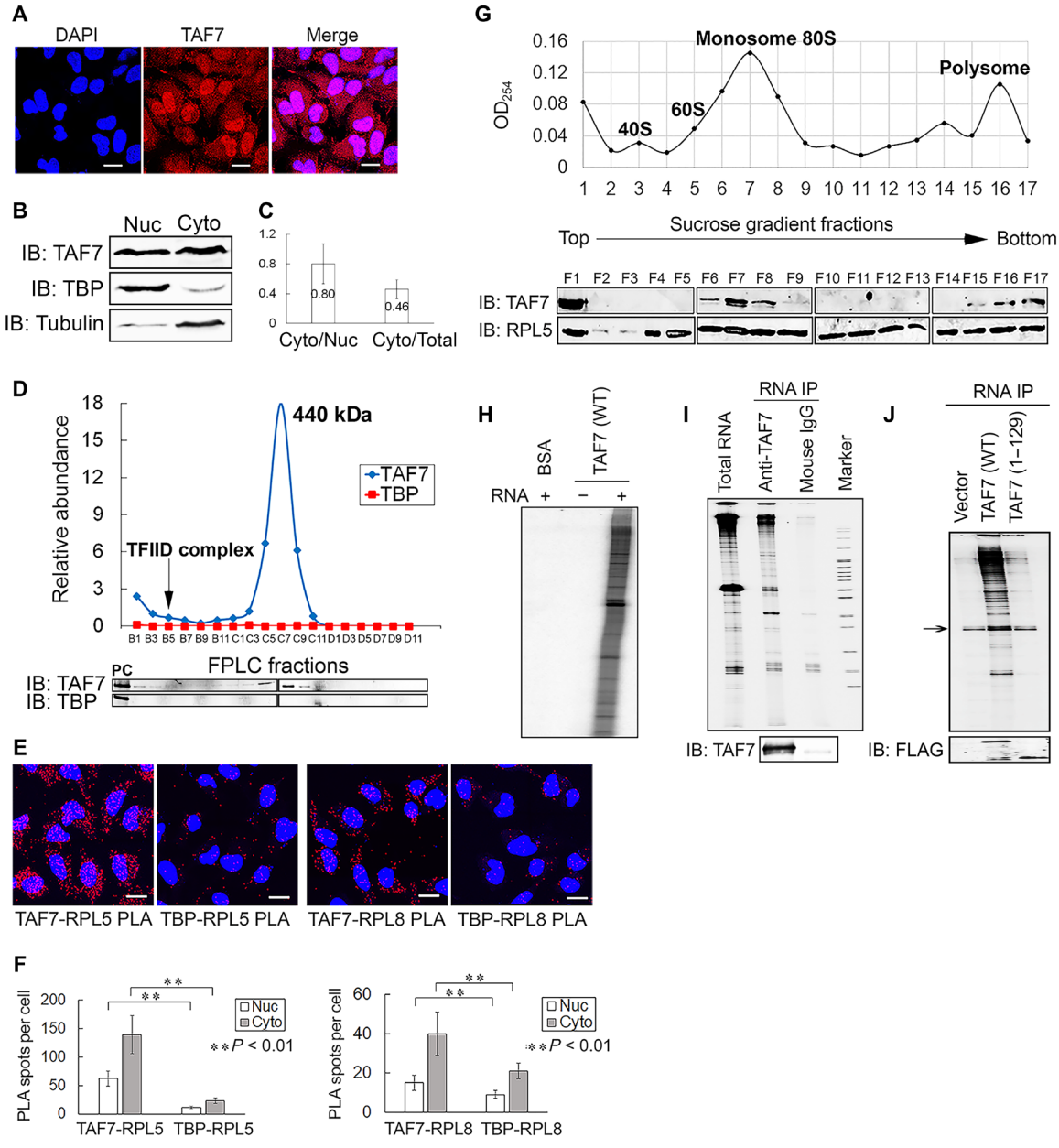

Fig. 1. TAF7 localizes in both the nucleus and the cytoplasm; cytoplasmic TAF7 is associated with RNA polysomes. (**A**) Immunofluorescence of TAF7 with anti-TAF7 (red) and DAPI (nuclear stain, blue) in HeLa cells. Scale bars, 10 μm. (**B**) Anti-TAF7 immunoblotting in HeLa nuclear and cytoplasmic fractions. Nuclear TBP and cytoplasmic β-tubulin assessed purity of respective fractions. (**C**) Enrichment of cytoplasmic TAF7 in HeLa cells as described in Materials and Methods. Error bars, means ± SD from three independent experiments. (**D**) FPLC column fractionation of HeLa cytoplasmic TAF7. HeLa TAF7 (WT) cytoplasmic extracts were subjected to Superose 6 gel-filtration chromatography; relative abundance of TAF7 and TBP in each fraction was calculated from results of immunoblotting with anti-TAF7 and anti-TBP. PC: recombinant TAF7 or TBP. (**E**) Proximity ligation assays (PLA) of TAF7 with RPL5 and RPL8. PLA associations, red spots; nuclear DAPI stain, blue. Scale bars, 10 μm. (**F**) Quantitation of PLA associations. PLA spots per cell were calculated on 400 to 500 cells. Data are means ± SD, $^{**}P < 0.01$. (**G**) Polysome fractionation of HeLa TAF7 (WT) cytoplasmic extracts. Cytoplasmic extracts, treated with RNase inhibitor, were subjected to sucrose gradient centrifugation; fractions were analyzed by immunoblotting with anti-TAF7 and anti-RPL5 (bottom). (**H**) TAF7 binds RNA in vitro. Recombinant TAF7 was incubated with HeLaS3 total RNA and immunoprecipitated with anti-TAF7. BSA was the control. Precipitated RNAs were ^{32}P 3′ end-labeled and resolved in RNA gels. (**I**) TAF7 binds RNA in cellulo. HeLa TAF7(WT) extracts were immunoprecipitated with anti-TAF7 or control mouse IgG. Precipitated RNA was 3′ end-labeled and resolved in RNA gels. Bottom, TAF7 recovery in the IP. (**J**) Truncation of TAF7 at amino acid 129 abrogates RNA binding in cellulo. Extracts from HeLaS3 cells expressing empty vector, TAF7 (WT), or TAF7 (1 to 129) were immunoprecipitated with anti-FLAG. TAF7-bound RNAs were 3′ end-labeled and examined in RNA gels. Arrow, nonspecific band. Bottom, FLAG-TAF7 recovery.

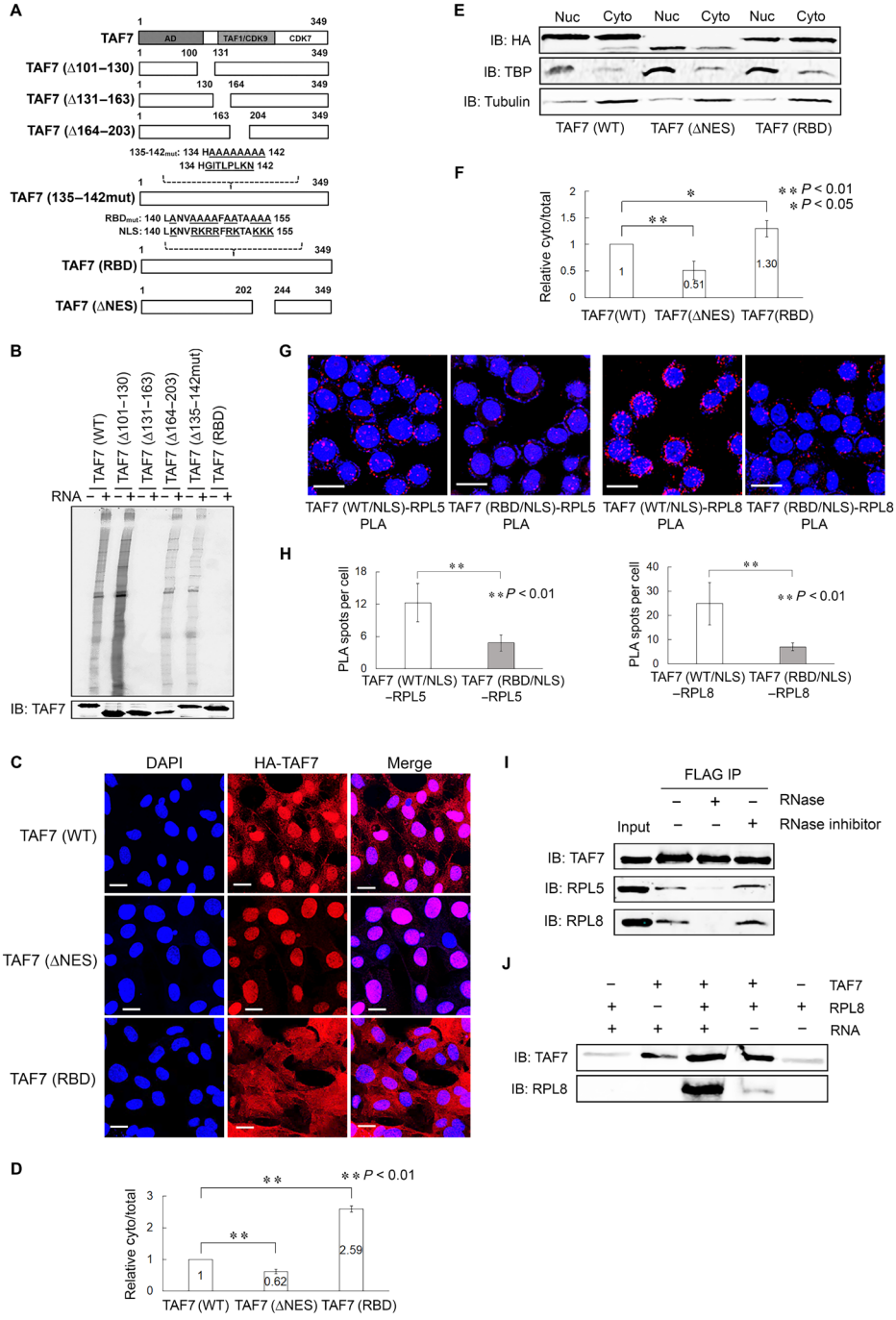

Fig. 2. TAF7 contains an RBD and nuclear localization and nuclear export signals. (**A**) Schematic showing TAF7 domains [activation domain (AD), domains phosphorylated by TAF1/CDK9 and CDK7], RBD, nuclear localization signal (NLS), nuclear export signal (NES), and locations of deletions and mutations. Residues mutated to alanine are underlined. (**B**) Mapping of TAF7 RBD. TAF7 mutants were incubated in vitro with HeLa S3 total RNA and immunoprecipitated with anti-TAF7 antibody. Recovered RNAs were 3′ end-labeled with ^{32}P and examined in an RNA gel. Bottom, TAF7 recovery. (**C**) Immunofluorescence with anti-HA antibody of TAF7 (WT), TAF7 (ΔNES), and TAF7 (RBD) (red) and DAPI (nuclear stain, blue) in MEF cells overexpressing HA-tagged TAF7 proteins. Scale bars, 10 μm. (**D**) Quantitation of HA-TAF7 immunofluorescence showing enrichment of TAF7 (RBD) and TAF7 (ΔNES) in the cytoplasm and nucleus, respectively. Ratios of cytoplasmic TAF7 to total TAF7 were calculated on >300 cells. Error bars, means ± SD, $^{**}P < 0.01$. (**E**) Immunoblotting (IB) analysis of TAF7 (WT), TAF7 (ΔNES), and TAF7 (RBD) in nuclear and cytoplasmic fractions from MEFs overexpressing HA-tagged proteins. (**F**) Determination of cytoplasmic enrichment of TAF7 (WT), TAF7 (ΔNES), and TAF7 (RBD) in MEFs overexpressing HA-tagged proteins. Cytoplasmic/total ratios of TAF7 were calculated from three independent experiments. Error bars, means ± SD, $^{**}P < 0.01$, $^{*}P < 0.05$. (**G**) PLA between TAF7 and RPL5 and RPL8 in HeLa cells expressing TAF7 (WT/NLS) and TAF7 (RBD/NLS). Red spots, PLA reactions; DAPI (blue), nucleus; scale bars, 10 μm. (**H**) Quantitation of PLA. PLA spots per cell were calculated on 500 to 600 cells for each interaction. Data are means ± SD, $^{**}P < 0.01$. (**I**) FLAG-IP of HeLa TAF7 (WT) cells in the presence of RNase inhibitor or RNase followed by immunoblotting. Cytoplasmic lysates were input. (**J**) TAF7 interacts with RPL8 in vitro. Recombinant FLAG-TAF7 was used to pull down rRPL8 protein in the presence and absence of RNA, respectively.

the nuclear localization of the TAF7 RBD mutant, TAF7 (RBD), in which the critical lysine and arginine residues that define an NLS had been replaced by alanine. The TAF7 (RBD) showed markedly reduced nuclear localization (Fig. 2, C to F). These results identify a TAF7 NLS between 140 and 155 that mediates nuclear import. The NLS overlaps the RBD. Therefore, we conclude that the TAF7 RBD maps to amino acids 141 to 155 and overlaps the TAF7 NLS.

Our discovery of TAF7 in the cytoplasm could reflect either de novo synthesized protein destined for transport into the nucleus or preexisting nuclear protein that had been actively transported out of the nucleus into the cytoplasm by an NES. To distinguish between these possibilities, we next determined whether TAF7 contains an NES. To this end, we examined additional truncation mutants. In contrast to the TAF7 (1 to 129) mutant, which is entirely cytoplasmic, the TAF7 (1 to 202) truncation is localized entirely to the nucleus (fig. S2, D and E), indicating the presence of an NES element between amino acids 203 and 349. A TAF7 (1 to 243) truncation mutant localized to both the nucleus and the cytoplasm, mapping a TAF7 NES to the C terminus between amino acids 203 and 243 (fig. S2, D and E). To further map and validate the putative NES, we constructed a mutant spanning the predicted TAF7 NES from amino acids 203 to 243, TAF7 (ΔNES) (Fig. 2A). As predicted, TAF7 (ΔNES) localized predominantly to the nucleus, whether assessed by immunofluorescence or cell fractionation (Fig. 2, C to F). Therefore, TAF7 has an NES between 203 and 243 that mediates export of TAF7 from the nucleus. These findings indicate that the observed cytoplasmic localization of TAF7 results in large part from the export of preexisting nuclear TAF7 into the cytoplasm.

TAF7 association with polysomes is mediated by RNA

The above results demonstrate that TAF7 directly interacts with RNA through an RBD. However, they do not exclude the possibility that TAF7's association with polysomes is through a direct interaction with ribosomal proteins. If the in situ colocalization of TAF7 with RPL5 and RPL8 observed in PLA is direct, then it should not be affected by mutation of the TAF7 RBD. However, if it is indirect and RNA dependent, the TAF7 RBD mutant should not colocalize with these ribosomal proteins. To distinguish between these possibilities, HeLa cells were transfected with either the TAF7 (WT/NLS) or TAF7 (RBD/NLS) mutant and examined by PLA. [Since mutation of the RBD also disrupts the TAF7 NLS, the SV40 (simian virus 40) NLS was fused to the N terminus of both the TAF7 (RBD) mutant and TAF7 (WT) to restore nuclear localization.] Whereas the WT TAF7 colocalized with RPL5 and RPL8, the TAF7 RBD mutant was no longer able to do so, suggesting that colocalization is mediated by RNA (Fig. 2, G and H).

To further examine whether the association of TAF7 with ribosomal proteins is mediated only by RNA, the ability of TAF7 to coimmunoprecipitate RPL5 and RPL8 was examined in HeLa cell extracts pretreated with ribonuclease (RNase) or RNAsin, or untreated. If the association of TAF7 with RPL5 or RPL8 is mediated by only RNA, then RNase pretreatment should disrupt the co-IP. Following RNase A pretreatment of HeLa cell extracts, TAF7 no longer coimmunoprecipitated either RPL5 or RPL8 (Fig. 2I). Conversely, an RNase inhibitor, RNasin, enhanced the co-IP, demonstrating that the association of TAF7 with RPL5 and RPL8 is RNA dependent (Fig. 2I). Furthermore, in in vitro pull-down assays using bacterially expressed recombinant FLAG-TAF7 proteins and RPL8 proteins, FLAG-TAF7 efficiently pulled down RPL8 in the presence of RNA, but not in its absence (Fig. 2J). FLAG-TAF7 also pulled down recombinant RPL5; the addition of RNase disrupted the interaction, whereas addition of the RNase inhibitor enhanced the interaction (fig. S2F). Therefore, the association of TAF7 with ribosomal proteins is mediated by RNA.

TAF7 binds a broad spectrum of RNA species at a 3′UTR CUG motif

The finding that TAF7 binds RNA led to the question of the nature of the RNA species it targets. To identify the RNAs bound by TAF7, we immunoprecipitated cytoplasmic RNA from HeLa TAF7 (WT) cells with an anti-FLAG antibody, followed by high-throughput RNA sequencing (RNA-seq) [RNA IP sequencing (RIP-seq)]. In two biological replicates of RIP-seq, we identified a common set of 936 immunoprecipitated RNAs with more than twofold enrichment in the FLAG-RIP relative to total RNA (Fig. 3, A and B). We also performed RIP-seq in HeLa TAF7 (WT) cells using an anti-TAF7 antibody and identified a total of 774 genes with more than twofold enrichment in TAF7-RIP relative to total RNA (fig. S3, A and B). Gene Ontology (GO) analysis of TAF7-bound RNAs did not identify specific functional categories. Rather, TAF7-bound RNAs fell into numerous categories of cellular process and function. Consistent with the RNAs falling into a range of functional categories, the length distribution of the immunoprecipitated RNA species largely paralleled that of the total RNA (fig. S3, C and D). These results provide direct evidence that TAF7 binds a broad spectrum of cellular RNAs.

A comparison of the RNA species bound by TAF7 with published chromatin IP–sequencing data (GSM803501) revealed a significant overlap between the genes whose transcription is regulated by TAF7 and the binding of their transcripts to TAF7 (fig. S3E). To determine whether TAF7 binds to a specific RNA sequence motif, we performed photoactivatable ribonucleoside–enhanced cross-linking and immunoprecipitation (PAR-CLIP) (*17*, *18*). In PAR-CLIP, 4-thiouridine (4SU) incorporation and ultraviolet (UV) irradiation lead to a specific and diagnostic T-to-C conversion in the cDNA libraries, thereby identifying the sites of RNA-protein interaction. PAR-CLIP was carried out in HeLa TAF7 (WT) cells using an anti-FLAG antibody. RNA fragments bound to cytoplasmic TAF7 were isolated and sequenced. Metagene analysis of the distribution of T-to-C conversions in three independent PAR-CLIP experiments indicated that cytoplasmic TAF7-binding sites were significantly enriched in the 3′UTR of mRNA (Fig. 3C).

Sequence-structure motif analysis of the PAR-CLIP data using the ssHMM analysis package (*19*) indicated that TAF7 binds the sequence motif CUG (fig. S3F) and that the preferential binding of TAF7 to CUG sequences is consistent with its binding to a broad spectrum of RNA species. To examine the potential structures of the sequences bound by TAF7, we analyzed the secondary structure of PAR-CLIP RNA fragments containing CUG using the RNAfold web server (*20*). The structural analyses did not reveal a predominant common structural motif, although a bias to CUG within a bulge was noted (fig. S3G). The results suggest that the basis of TAF7 specificity in its binding to RNA is dominated by the CUG motif located within a bulge.

One of the most notable examples of RNA species with a CUG motif in a bulge is the HIV-1 transactivation response (TAR) RNA. The structure of the HIV-1 TAR RNA sequence, and its binding by the HIV-1 transactivator, Tat, has been extensively characterized.

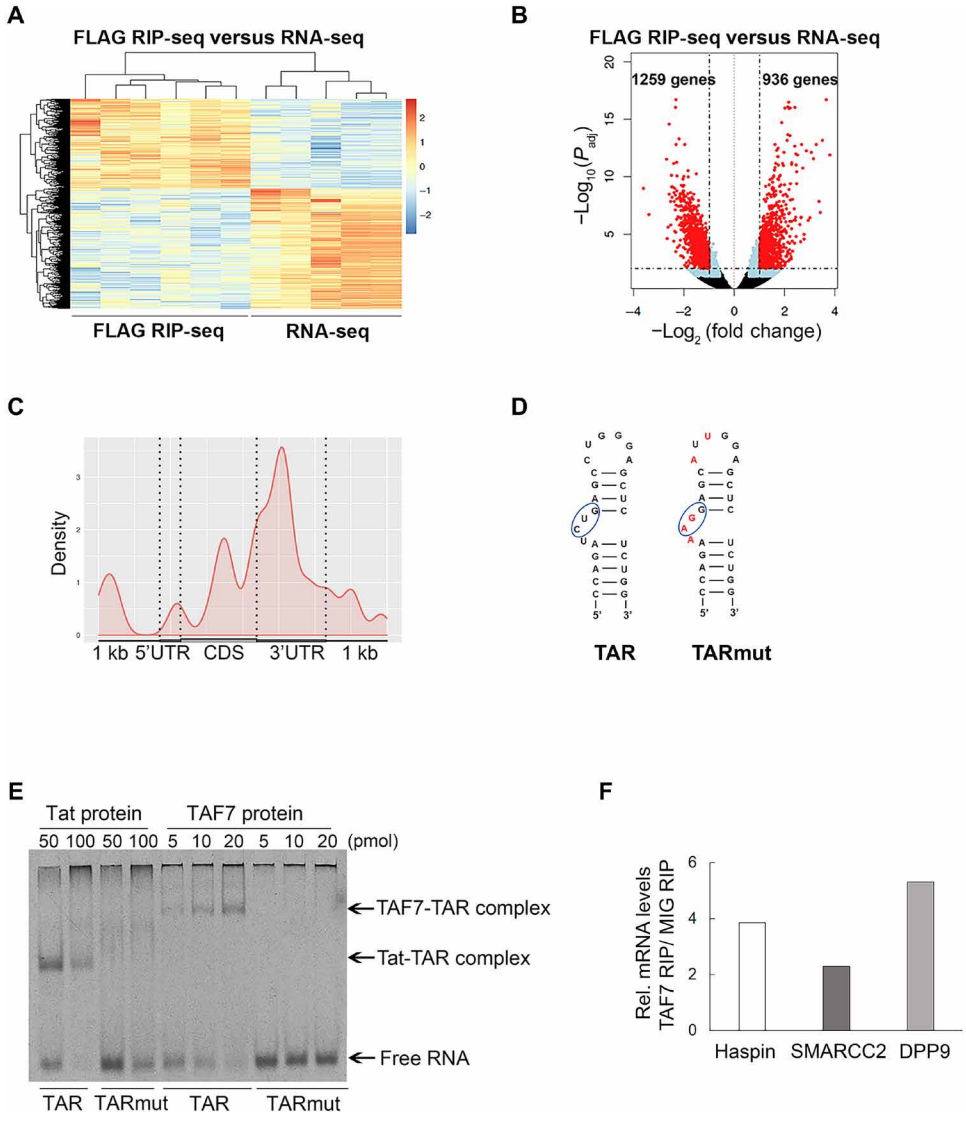

Fig. 3. TAF7 binds a broad spectrum of RNA species. (**A**) Heatmap displaying the differential expression patterns of genes (with a fold change >2 and P_{adj} <0.01) in FLAG RIP-seq and RNA-seq of HeLa TAF7 (WT). (**B**) Volcano plot of mRNA expression in FLAG RIP-Seq versus RNA-seq of HeLa TAF7 (WT) cells. Genes with a fold change > 2, and P_{adj} < 0.01 are labeled in red. (**C**) Metagene analysis of PAR-CLIP T-to-C mutation site distribution across mRNA features, including 5′UTR, CDS (Coding Sequence), and 3′UTR. (**D**) Structure of TAR RNA with sites of mutation indicated in red. (**E**) TAF7-TAR interaction by EMSA. Increasing amounts of purified HIV-1 Tat proteins (50 and 100 pmol) or TAF7 proteins (5 , 10 , and 20 pmol) were incubated with WT or mutant TAR RNA (TARmut). The bands corresponding to free RNA and Tat-TAR and TAF7-TAR complexes are indicated by arrows. (**F**) Haspin mRNA, SMARCC2 mRNA, and DPP9 mRNA were immunoprecipitated with TAF7 in HeLa cells. The abundance of mRNA immunoprecipitated by TAF7 was measured in real-time PCR and compared with the abundance of mRNA immunoprecipitated by control mouse IgG. Results are representative of three independent experiments with a minimum of two technical replicates per experiment.

It consists of a stem-loop, with a CUG located in a bulge within the stem that is required for Tat binding (Fig. 3D). Mutation of the CUG motif eliminates Tat binding (Fig. 3, D and E). On the basis of our finding that the TAF7 recognition motif is enriched in the CUG trinucleotide, we predicted that TAF7 would bind to HIV-1 TAR RNA and that binding would be CUG dependent. As assessed by electrophoretic mobility shift assays (EMSAs), TAF7 bound to the native TAR sequence (Fig. 3E). Mutation of the Tat binding site completely abrogated binding of both TAF7 and Tat. These results clearly demonstrate that TAF7 binding to RNA is sequence specific.

The above studies used HeLa cells stably expressing exogenous FLAG-TAF7. To validate the predicted interactions between TAF7 and its target RNAs, endogenous TAF7 was immunoprecipitated from HeLa cells. Coimmunoprecipitated RNA was then probed for the presence of three target RNAs, namely, Haspin, SMARCC2, and DPP9, that were predicted from the HeLa TAF7 (WT) PAR-CLIP data. In three independent experiments, all three RNA species were enriched in TAF7 coimmunoprecipitates (Fig. 3F). Thus, the RNA targets predicted by the exogenous TAF7 RIP-seq experiments are validated by endogenous TAF7 binding.

TAF7 is actively exported to the cytoplasm through an XPO1-dependent pathway

The above results demonstrate that TAF7 is an RNA binding protein that localizes to both the nucleus and the cytoplasm. The identification of a TAF7 NES further suggests that TAF7 is actively exported from the nucleus to the cytoplasm. Therefore, we next asked whether TAF7 nuclear export is mediated by exportin 1 (XPO1), which is a major nuclear export receptor. To address this question, we analyzed the effect of leptomycin B (LMB), an XPO1 inhibitor, on the subcellular localization of TAF7. If TAF7 nuclear export depends on XPO1, LMB treatment should result in a retention of TAF7 in the nucleus. Short-term treatment of HeLa cells with LMB resulted in an increase of 40.1% in nuclear accumulation of TAF7, as assessed by either immunofluorescence or immunoblotting of fractionated cells (Fig. 4, A to C). Thus, XPO1 mediates TAF7 export from the nucleus.

The direct association of XPO1 with TAF7 was demonstrated both in situ and in vitro. PLA detected robust XPO1-TAF7 association (Fig. 4, D and E, and fig. S4A). In contrast, neither the nuclear protein hnRNP U nor the cytoplasmic protein eIF5B, which served as negative controls, colocalized with XPO1, as assessed by PLA (Fig. 4, D and E, fig. S4, B and C). In addition, XPO1 coimmunoprecipitated with TAF7 in both HeLa nuclear and cytoplasmic extracts (fig. S4D). Together, these data demonstrated that XPO1 actively exports TAF7 out of the nucleus.

TAF7 contributes to cytoplasmic export of target RNAs and the regulation of their translation

The finding that TAF7 binds RNA and is exported to the cytoplasm led to the prediction that export of TAF7-target RNAs depends on their binding to TAF7. To test this prediction, we asked whether mutation of the TAF7 RBD leads to nuclear accumulation of target RNA species. The TAF7 (WT/NLS) and TAF7 (RBD/NLS) constructs (described above) were introduced into mouse embryonic fibroblasts (MEFs), in which the TAF7 locus is flanked by flox sites (MEF TAF7$^{fl/fl}$) and the endogenous TAF7 was deleted by Cre. Both the TAF7 (RBD/NLS) and the TAF7 (WT/NLS) proteins were expressed in MEFs and localized to both nucleus and cytoplasm (fig. S5A). No significant differences were observed in total RNA synthesis, as measured by 5-fluorouridine (5-FU) incorporation, between the MEFs containing TAF7 (WT/NLS) and those with TAF7 (RBD/NLS) (fig. S5B). Thus, the RBD does not appear to be necessary

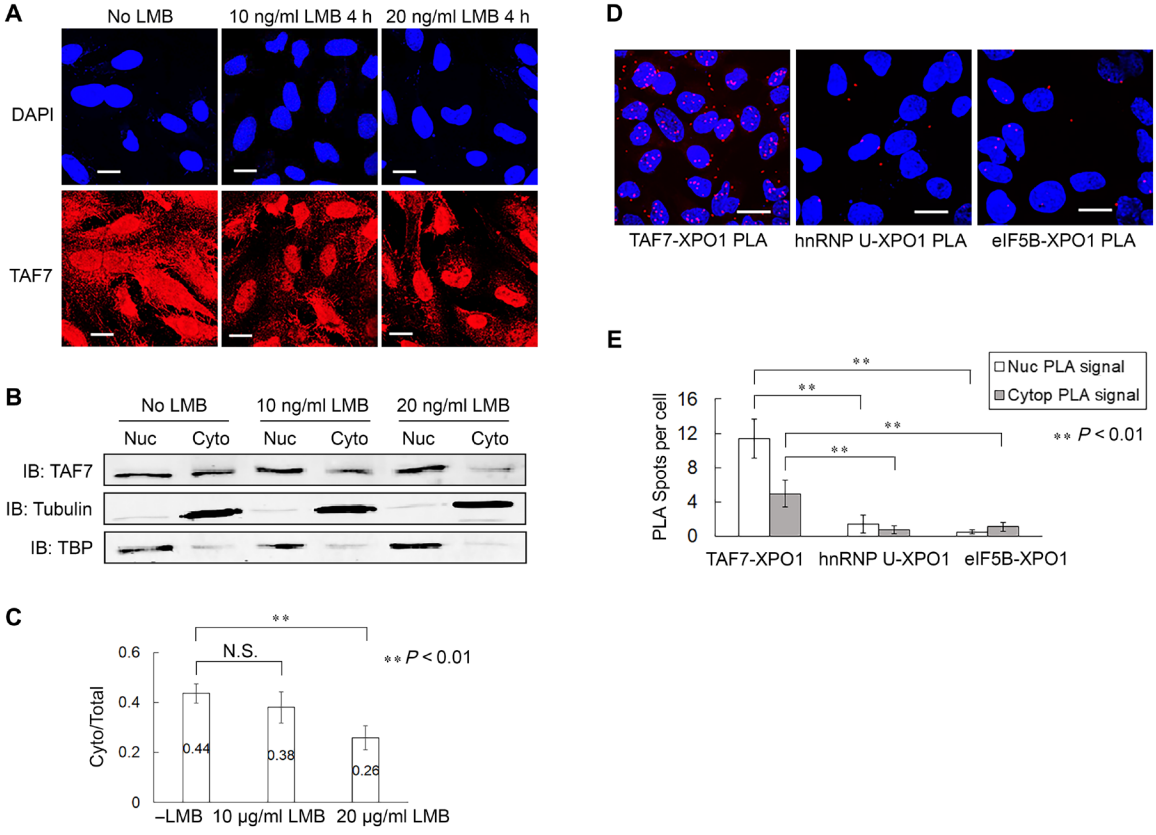

Fig. 4. TAF7 is actively exported to the cytoplasm through an XPO1-dependent pathway. (**A**) Immunofluorescence with anti-TAF7 antibody indicating subcellular localization of TAF7 (red) in HeLa cells following leptomycin B (LMB) treatment. DAPI stains the nucleus, and scale bars indicate 10 μm. (**B**) IB analysis with anti-TAF7 antibody of TAF7 in nuclear and cytoplasmic fractions from HeLa cells following a 4-hour treatment with or without LMB. The nuclear protein TBP and the cytoplasmic protein tubulin were used as controls. (**C**) Quantitation of the effect of LMB treatment on the cytoplasmic/total TAF7 ratio. The ratios are calculated from three independent immunoblotting experiments. Error bars indicate mean ± SD, $^{**}P < 0.01$. N.S., not significant. (**D**) PLA revealing the in situ interaction of XPO1 with TAF7, but not with nuclear hnRNP U or cytoplasmic eIF5B. The red spots indicate PLA reactions, DAPI stains the nucleus, and scale bars indicate 10 μm. (**E**) Quantification of PLA colocalizations. PLA spots per cell were calculated on 400 to 500 cells for each PLA interaction. Data are presented as means ± SD, $^{**}P < 0.01$.

for TAF7's function in transcription. To determine whether the RBD mutation affected RNA export, we examined the localization of three of the RNAs identified by PAR-CLIP as binding to TAF7, namely, Haspin, SMARCC2, and DPP9. Consistent with the prediction, mutation of the TAF7 RBD resulted in an accumulation of RNA in the nucleus (fig. S5C). These findings are consistent with the interpretation that TAF7 mediates export of its target RNA species from the nucleus.

To further examine the role of TAF7 in RNA export, the TAF7 (RBD/NLS) mutant was introduced into HeLa cells following knockdown of endogenous TAF7 by a small interfering RNA (siRNA) targeted to the RBD; introduction of TAF7 (WT/NLS) following treatment with a nontargeting siRNA served as a control (fig. S5D). The nuclear/cytoplasmic localizations of Haspin, SMARCC2, and DPP9 RNAs were compared between the TAF (RBD/NLS) and TAF7 (WT/NLS) cells (Fig. 5A). In cells expressing the TAF7 (RBD/NLS) mutant, all three RNA species were significantly retained in the nucleus, supporting the conclusion that TAF7 transports its bound RNAs to the cytoplasm.

As described above, TAF7 binds to the TAR sequence within the HIV-1 long terminal repeat (LTR), leading to the prediction that cytoplasmic shuttling of transcripts encoded by the LTR would be mediated by TAF7 (WT) but not by the TAF7 (RBD) mutant, which would result in nuclear retention. To test this prediction, HeLa cells in which endogenous TAF7 was replaced by either TAF7 (RBD/NLS) or TAF7 (WT/NLS) were transiently transfected with an HIV-1 LTR-luciferase construct, and the distribution of luciferase RNA between nucleus and cytoplasm was assessed. Compared with the TAF7 (WT/NLS), the TAF7 (RBD/NLS) led to a marked 5.5-fold increase in nuclear retention of the LTR-encoded transcript (Fig. 5B). Therefore, the binding of TAF7 to the LTR TAR sequence mediates its transport to the cytoplasm.

The above findings indicate that TAF7 binds and transports RNA to the cytoplasm, where it robustly associates with polysomes. This led us to speculate that TAF7 contributes to the regulation of translation through its transport of RNA. The effect on protein synthesis of the TAF7 (RBD/NLS) mutant was first determined using the surface sensing of translation (SUnSET) assay, a nonradioactive puromycin-labeling method used to assess protein synthesis (*21*). As measured by fluorescence-activated cell sorting (FACS) analysis of puromycin incorporation, cells expressing TAF7 (RBD/NLS) had significantly decreased puromycin incorporation, and thus total protein synthesis, relative to cells expressing TAF7 (WT/NLS) in MEFs (Fig. 5C). Synthesis of the products of TAF7's RNA targets was similarly affected. Thus, HeLa cells expressing TAF7 (RBD/NLS) had markedly lower levels of Haspin, DPP9, and SMARCC2, as determined by immunoblotting analysis of cell extracts (Fig. 5, D to F). Therefore, optimal translation depends on the cytoplasmic export by TAF7 of its target RNAs.

To further examine the role of TAF7 in translation, we determined the effect on protein synthesis of blocking nuclear export of TAF7. The TAF7 (ΔNES) mutant is able to bind RNA but largely unable to translocate to the cytoplasm (Fig. 2, C to F). We predicted that the TAF7 (ΔNES) mutant, like the TAF7 (RBD) mutant, would result in reduced protein synthesis. Endogenous TAF7 was knocked down in HeLa cells using antisense RNA specific for the segment deleted in the TAF7 (ΔNES) mutant and replaced with exogenous TAF7 (ΔNES) mutant; exogenous WT TAF7 introduced into HeLa cells treated with a nontargeting siRNA served as control. We also examined translation in MEF TAF7$^{fl/fl}$ cells in which endogenous TAF7 was deleted with Cre and replaced with either TAF7 (ΔNES) or WT TAF7 (fig. S6, A to C). Endogenous TAF7 is efficiently removed, and exogenous TAF7 (ΔNES) mutant is largely localized to the nucleus (fig. S6B). To ensure that global transcription levels were unaffected by the TAF7 (ΔNES) mutant, the extent of 5-FU incorporation into nascent transcripts was determined. As shown in fig. S6 (D and E), there is no significant difference in global transcription in cells expressing TAF7 (ΔNES) relative to those rescued with WT TAF7 in either MEFs or HeLa cells.

The effect of depleting cytoplasmic TAF7 on protein synthesis was then examined by the SUnSet assay. Both MEFs and HeLa cells expressing TAF7 (ΔNES) had significantly decreased puromycin incorporation relative to cells expressing TAF7 (WT) (Fig. 6, A and B). To further examine the contribution of TAF7 to translation, we assessed the effect of the TAF7 (ΔNES) mutant on the levels of protein encoded by specific RNA species bound by TAF7. To this end, we again examined Haspin, SMARCC2, and DPP9. The levels of each of the three proteins in cellular extracts from MEF cells expressing only exogenous TAF7 (ΔNES) or TAF7 (WT) were determined by immunoblotting (Fig. 6, C to E). Consistent with the SUnSET data, depletion of TAF7 from the cytoplasm resulted in reduced levels of all three proteins, although to differing degrees. The reduction in protein levels could not be attributed to reduced transcripts since the levels of RNA encoding these three proteins did not differ (fig. S6, F to H). The basis for the difference among the three proteins remains to be determined but may reflect differences in their half-lives. These findings lead to the conclusion that TAF7 contributes to the regulation of protein synthesis. Together, these results demonstrate that TAF7 regulates translation through a mechanism in which it binds to a spectrum of target RNA species and transports them to, and remains associated with, cytoplasmic polysomes for optimal translation.

DISCUSSION

Initially characterized as a component of the general transcription factor TFIID, TAF7 is now understood to have pleiotropic functions in transcription: It functions to regulate each step in transcription initiation and elongation. The importance of TAF7 in regulating transcription is underscored by the fact that germline disruption of the TAF7 gene is embryonically lethal; in primary cells and cell lines, TAF7 is essential for proliferation (*13*). The present studies extend the importance of TAF7 in regulating cellular homeostasis by showing that TAF7 is an RNA binding factor that transports RNA into the cytoplasm, where it is associated with polysomal mRNA and contributes to the regulation of translation. Protein synthesis and levels of the protein products of TAF7's RNA targets are reduced by either depletion of cytoplasmic TAF7 or loss of TAF7 RNA binding. On the basis of these findings, we propose a model in which TAF7 is a pleiotropic regulator of gene expression, linking the processes of transcription, mRNA export, and translation (Fig. 7).

TAF7 is an RNA binding protein

TAF7 has an RBD located in the center of the molecule, between amino acids 141 and 155. It binds a broad spectrum of RNA species, primarily at CUG motifs located at bulges in stem structures within the 3′UTR. Its binding to many different RNA species is consistent with the requirement for TAF7 in transcription of 65% of expressed

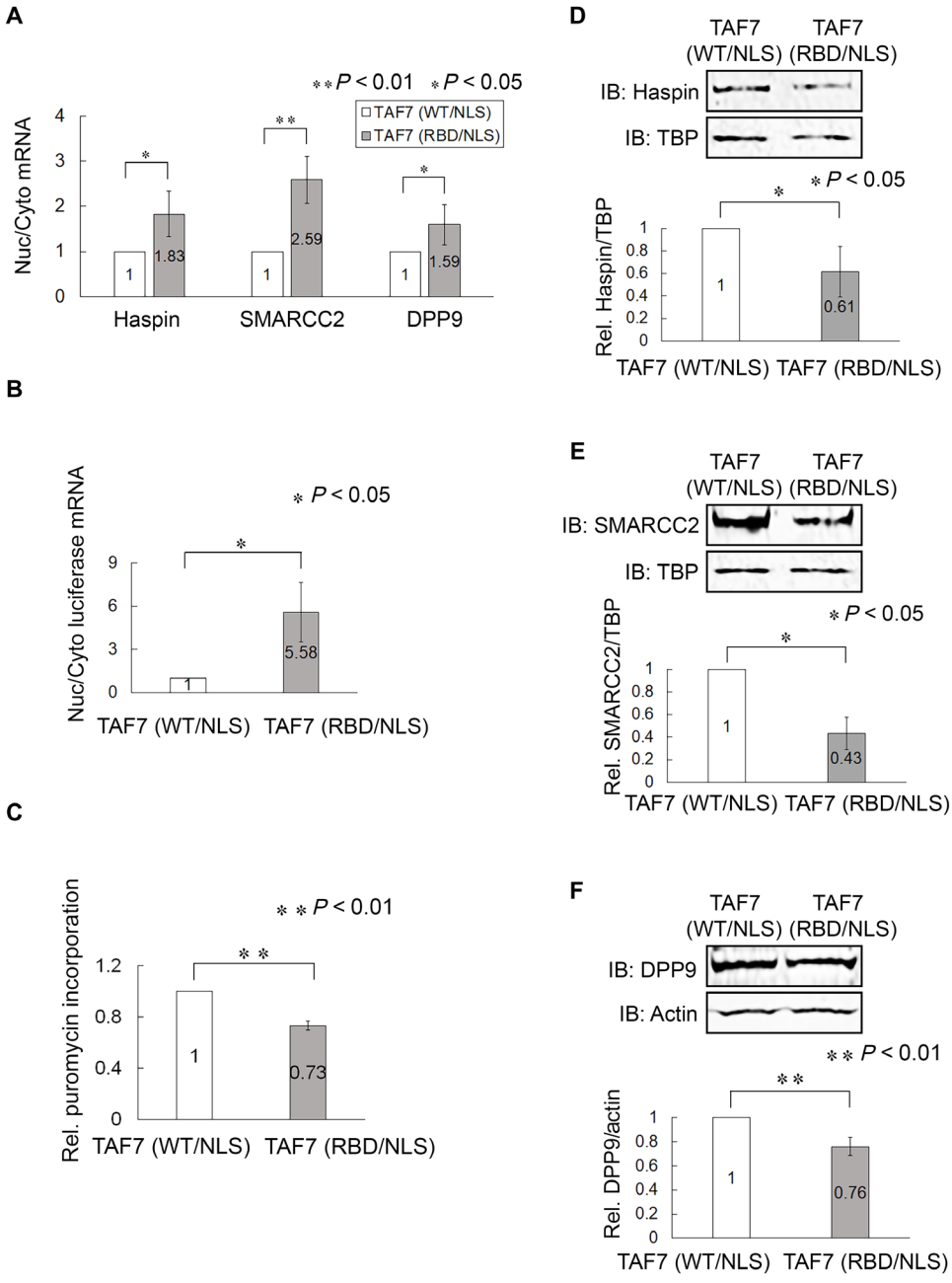

Fig. 5. Disruption of TAF7 RBD leads to a retention of TAF7 RNA targets in the nucleus and a reduction of protein synthesis from TAF7 RNA targets. (**A**) Mutation of TAF7 RBD impaired export of RNA targets. TAF7 (RBD/NLS) mutant and TAF7 (WT/NLS) were transduced into HeLa cells depleted of endogenous TAF7 by siRNA. Nuclear and cytoplasmic levels of Haspin, SMARCC2, and DPP9 mRNAs were measured by real-time PCR. Nuclear/cytoplasmic mRNA ratios were calculated from at least three independent experiments with a minimum of two technical replicates per experiment. Data are means ± SD, $^{**}P < 0.01$, $^{*}P < 0.05$. (**B**) Export of HIV-1 LTR-luciferase RNA is impaired in TAF7 RBD mutant. HIV-1 LTR-luciferase construct was transiently transfected into HeLa TAF7 (WT/NLS) and HeLa TAF7 (RBD/NLS) cells depleted of endogenous TAF7 by siRNA. Nuclear and cytoplasmic levels of luciferase mRNAs were measured by real-time PCR. Nuclear/cytoplasmic mRNA ratios were calculated from three independent experiments with a minimum of two technical replicates per experiment. Data are means ± SD, $^{*}P < 0.05$. (**C**) Protein synthesis is reduced with TAF7 RBD mutant. TAF7 (RBD/NLS) mutant and TAF7 (WT/NLS) were transduced into MEF TAF7$^{fl/fl}$ cells depleted of endogenous TAF7 by Cre and protein synthesis measured by SUnSET. Results are shown as relative puromycin incorporation in MFI. Data are means ± SD, $^{**}P < 0.01$. (**D** to **F**) IB analysis of Haspin, SMARCC2, and DPP9 levels in HeLa TAF7 (WT/NLS) + siRNA and HeLa TAF7 (RBD/NLS) + siRNA extracts. TBP was used as a control for Haspin and SMARCC2 in nuclear extracts; actin was used as a control for DPP9 in total cell extracts. Error bars indicate means ± SD from three independent experiments, $^{**}P < 0.01$, $^{*}P < 0.05$.

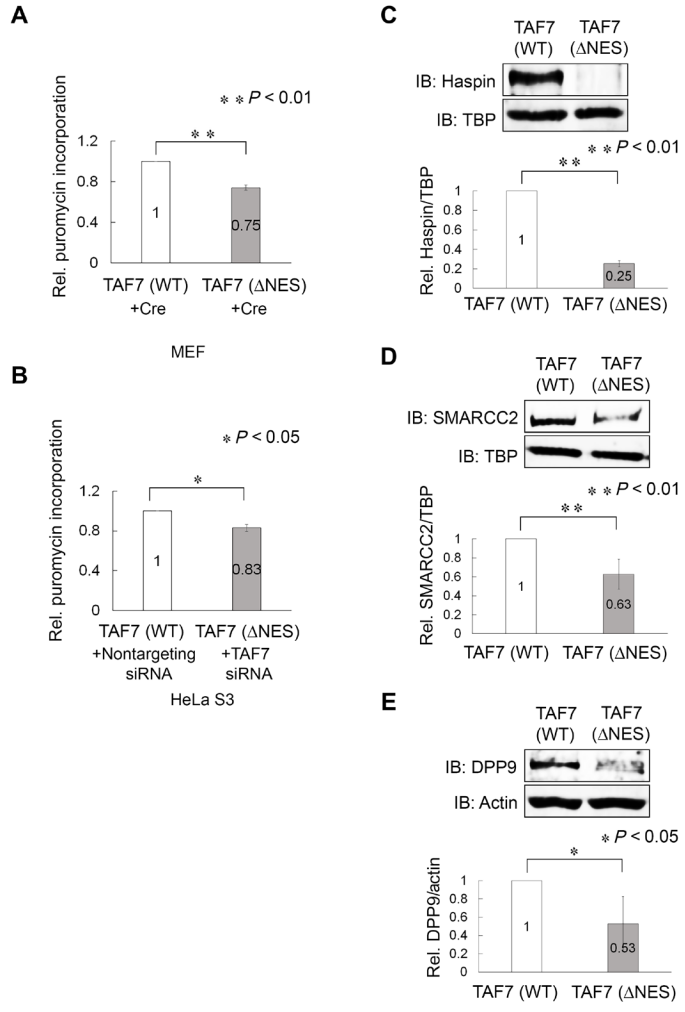

Fig. 6. Depletion of cytoplasmic TAF7 leads to a reduction of protein synthesis from TAF7 RNA targets. (**A**) SUnSET analysis of global protein synthesis in MEF TAF7$^{fl/fl}$ cells depleted of endogenous TAF7 by Cre and overexpressing TAF7 (WT) or TAF7 (ΔNES). Following puromycin (10 μg/ml) treatment as described, incorporation was calculated from FACS analysis of puromycin-labeled cells. Data are presented as means ± SD, $^{**}P < 0.01$. (**B**) SUnSET analysis of global protein synthesis in HeLa S3 cells depleted of endogenous TAF7 by siRNA and overexpressing TAF7 (WT) or TAF7 (ΔNES). Following puromycin (10 μg/ml) treatment as described, incorporation was calculated from FACS analysis of puromycin-labeled cells. Data are presented as means ± SD, $^{*}P < 0.05$. (**C**) IB analysis of Haspin levels in MEF TAF7$^{fl/fl}$ TAF7 (WT) + Cre and MEF TAF7$^{fl/fl}$ TAF (ΔNES) + Cre nuclear extracts. TBP was used as a control. The Haspin/TBP values were calculated from three independent IB experiments. Error bars indicate means ± SD, $^{**}P < 0.01$. (**D**) IB analysis of SMARCC2 levels in MEF TAF7$^{fl/fl}$ TAF7 (WT) + Cre and MEF TAF7$^{fl/fl}$ TAF7 (ΔNES) + Cre nuclear extracts. TBP was used as a control. The SMARCC2/TBP values were calculated from three independent IB experiments. Error bars indicate mean ± SD, $^{**}P < 0.01$. (**E**) IB analysis of DPP9 levels in MEF TAF7$^{fl/fl}$ TAF7 (WT) + Cre and MEF TAF7$^{fl/fl}$ TAF7 (ΔNES) + Cre total cell extracts. Actin was used as a control. The DPP9/actin values were calculated from three independent IB experiments. Error bars indicate means ± SD, $^{*}P < 0.05$.

genes in rapidly proliferating cells (*12*). GO analyses of TAF7-bound RNAs identified categories of RNA associated with a variety of cellular pathways, including proliferation, cell cycle, metabolism, and cytoskeleton organization. Accordingly, mutation of the RBD results in a decrease in total protein synthesis. We conclude that TAF7 functions to chaperone the RNAs whose genes it regulates from the nucleus to the cytoplasm.

TAF7 binds HIV-1 TAR RNA

The RNA structure and sequence preference of TAF7 binding to RNA are remarkably similar to those of HIV-1 Tat, the transactivator protein for HIV-1. HIV-1 Tat is a well-established RNA binding protein that associates with HIV-1 TAR RNA and a specific set of viral mRNAs and host mRNAs (*22*–*25*). The RBD of Tat, like that of TAF7, is an arginine/lysine–rich basic region (*26*). Moreover, like TAF7, HIV-1 Tat binds RNAs at the junction between a pyrimidine bulge and an adjacent stem (*24*, *25*, *27*, *28*).

Although there is no structural similarity between TAF7 and Tat, there are other notable parallels between these two proteins. We have reported previously that HIV-1 Tat, like TAF7, binds TAF1 and inhibits its acetyltransferase activity (*5*, *7*). Furthermore, like HIV-1 Tat, TAF7 interacts with TFIIH and P-TEFb to regulate the phosphorylation of Pol II CTD (*10*, *29*, *30*). Extending the parallels between TAF7 and HIV-1 Tat, Tat functions as a transcription activator in the nucleus and facilitates translation of its own mRNA and other HIV-1 mRNAs in the cytoplasm (*24*, *31*, *32*). Together, these functional parallels suggest that TAF7 may be the mammalian homolog of HIV-1 Tat. They also lead to the speculation that TAF7 may be necessary for initiating HIV-1 infection.

TAF7 is a nucleocytoplasmic shuttling protein

Although TAF7 is a well-characterized transcriptional regulator in the nucleus, we have made the unexpected finding that TAF7 is also a cytoplasmic protein that is actively exported from the nucleus to the cytoplasm. While nuclear localization of TAF7 is mediated by its NLS, nuclear export is dependent on an NES. The NES-dependent export of nuclear TAF7 into the cytoplasm is mediated by the major nuclear export receptor XPO1 (*33*). The possibility that other export receptors also mediate TAF7 export has not been examined, although no interaction with nuclear RNA export factor 1 (NXF1) has been observed. XPO1 is known to use RNA binding proteins as adapters for RNA export. Examples include HIV-1 REV and hnRNP, as well as TFIIIA, which binds to and chaperones nuclear export of 5S ribosomal RNA (rRNA) in amphibian oocytes (*33*–*38*). Since TAF7 interacts with XPO1, and inhibition of XPO1 results in the retention of TAF7 in the nucleus, TAF7 appears to function as an adapter for XPO1-mediated transport of its RNA cargo.

Translation depends on RNA export by TAF7

In the cytoplasm, TAF7 contributes to translation. Thus, TAF7 is associated with a large 440-kDa complex that consists of ribosomal proteins; no other TFIID components are found within the complex. TAF7 is associated with polysomes through its interaction with RNA. Furthermore, retention of TAF7 in the nucleus, by mutation of its NES, results in a global decrease in translation and a decrease in the levels of proteins whose RNAs are bound by TAF7. Mutation of the TAF7 RBD similarly results in decreased global translation. Thus, a novel function of TAF7 is to deliver its RNA cargo to polysomes for translation. Consistent with TAF7 regulating transcription of and binding to a broad spectrum of RNA species, this seems to be a general function not restricted to a specific functional subset of transcripts.

TAF7 coordinates transcription and translation

The present studies provide evidence for the coordination of transcription and translation by the TFIID component, TAF7. We have

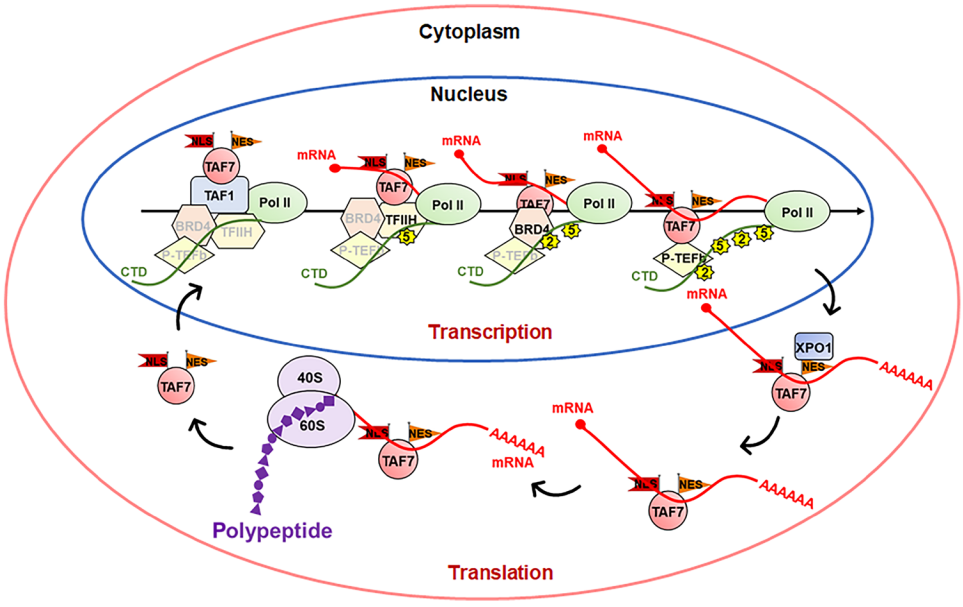

Fig. 7. Model for role of TAF7 in linking transcription and translation. In the nucleus, TAF7 acts as a checkpoint regulator of transcription through its regulation of the enzymatic activities of TAF1/TFIID, TFIIH/CDK7, BRD4, and P-TEFb/CDK9. TAF7 can also function as an RNA chaperone, binding RNA transcripts, and transporting them into the cytoplasm through an XPO1-dependent pathway. In the cytoplasm, TAF7 delivers its RNA cargo to polysomes to promote protein translation. Subsequent release of RNA from TAF7 reveals its NLS enabling the import of cytoplasmic TAF7 back to the nucleus.

shown that TAF7, which regulates each step in transcription initiation, also regulates translation. The mechanism by which TAF7 regulates translation is through its binding to and chaperoning of a broad spectrum of RNA species from the nucleus to the cytoplasm, delivering them to polysomes to promote global protein synthesis. On the basis of our findings, we propose a model in which TAF7 integrates transcription and translation machineries that operate in distinct cellular compartments (Fig. 7). In the nucleus, TAF7 regulates transcription through its regulation of the enzymatic activities of TAF1/TFIID, TFIIH, BRD4, and P-TEFb, traveling with the elongation complex. It then functions as an RNA chaperone, binding RNA and transporting it to the cytoplasm. In the cytoplasm, TAF7 delivers its RNA cargo to polysomes, thereby contributing to translation. Of note, the TAF7 NLS overlaps with its RBD: Deletion of the NLS abrogates RNA binding. In the cytoplasm, RNA bound to TAF7 would mask the NLS, preventing cytoplasmic TAF7-RNA complexes from being imported back into the nucleus. After delivering RNA to polysomes, TAF7 is released from the RNA, thereby exposing the NLS and enabling shuttling of TAF7 back to the nucleus. In conclusion, TAF7 is a multifunctional regulator of gene expression, which coordinates many of the complex steps of gene expression.

MATERIALS AND METHODS

Cell culture and generation of TAF7 cell lines

HeLa cells and MEFs were cultured in Dulbecco's modified Eagle's medium (DMEM) supplemented with 10% fetal bovine serum. MEF TAF7$^{f/f}$ cells were generated from TAF7$^{f/f}$ mice, which were described previously (*13*). HeLa S3 cell lines were cultured in F12K medium supplemented with 10% fetal bovine serum. Hela TAF7 (WT), TAF7 (1 to 202), TAF7 (1 to 243), and TAF7 (1 to 129) cell lines were described previously (*39*). HeLa TAF7 (ΔNES), HeLa TAF7 (WT/NLS), and HeLa TAF7 (RBD/NLS) cell lines were generated by retrovirus transduction described below.

Retrovirus production and transduction were as previously described (*13*). The corresponding TAF7 sequences (WT, ΔNES, RBD, WT/NLS, and RBD/NLS) without stop codon [for hemagglutinin (HA) tagging] were introduced in the murine stem cell virus (MSCV)–HA–internal ribosomal entry site–nerve growth factor receptor (NGFR) vector at the Bgl II site. The resulting MSCV-HA-TAF7-NGFR vectors were transfected into Plat E cells for retrovirus production. MEF TAF7$^{f/f}$ cells were transduced with 6 ml retrovirus/10^6 using polybrene and harvested 48 hours after infection. NGFR-positive cells were isolated by FACS. For conditional deletion of endogenous TAF7, the MEF TAF7$^{f/f}$ cells were transduced with retrovirus carrying Cre–green fluorescent protein (GFP). GFP-positive cells were purified by FACS.

Protein expression and purification

Expression plasmids for FLAG-tagged TAF7 (WT) and TAF7 mutants were described previously (*5*). Briefly, the corresponding TAF7 regions (Δ101 to 130, Δ130 to 163, Δ164 to 203, 135 to 142mut, and RBD) were polymerase chain reaction (PCR)–amplified and inserted between the Nde I and Bam HI sites in the pF:55-11d vector (*5*). Recombinant FLAG-TAF7 (WT) and derived mutants were expressed and purified from *Escherichia coli* BL21 cells using anti-FLAG M2 affinity gel (A2220, MilliporeSigma) as previously described (*5*).

Antibodies

Antibodies used for immunoblotting, IP, or immunofluorescence were as follows: anti-TAF7 (TAF7 monoclonal antibody M01, clone 2C5, Abnova); anti-TBP (ab63766, Abcam); anti–β-tubulin (ab6046, Abcam); anti-HA (16B12, ab130275, Abcam); anti-FLAG (clone M2, F3165, MilliporeSigma); anti-puromycin (clone 12D10, MABE343,

MilliporeSigma); anti-RPL5 (ab86863, Abcam); anti-RPL8 (ab169538, Abcam); anti-XPO1 (M01180, Boster); anti-eIF5B (ab89016, Abcam); anti-hnRNP U (ab20666, Abcam); anti-Haspin (ab21686, Abcam); anti-SMARCC2 (A301-039A, Bethyl); and anti-DPP9 (ab42080, Abcam). The specificity of the anti-TAF7 antibody for TAF7 has been shown previously using MEFs deleted of TAF7 (*13*).

Nuclear and cytoplasmic fractionation

The cells were washed with ice-cold phosphate-buffered saline, scraped from the dish, and then collected by low-speed centrifugation. Then, cells were lysed with lysis buffer [10 mM NaCl, 3 mM $MgCl_2$, 10 mM tris-HCl (pH 7.4), and 0.5% NP-40] on ice for 30 s, followed by centrifugation at 17,000*g* for 30 s at 4°C, which resulted in ~90% lysis. The supernatant was collected as cytoplasmic extracts. The pellet was then suspended in nuclear lysis buffer [20 mM Hepes (pH 7.9), 400 mM NaCl, 1 mM EDTA, and 10% glycerol], incubated for 2 hours at 4°C with rotation, and centrifugated at 17,000*g* for 5 min at 4°C. The supernatant was collected as nuclear extracts.

LMB treatment

For inhibition of XPO1-mediated nuclear export pathway, cells were incubated in medium supplemented with LMB (15 ng/ml; L2913, MilliporeSigma) for 4 hours. After incubation, cells were harvested and then lysed to generate nuclear and cytoplasmic extracts.

IP and immunoblotting

For FLAG IP, the cytoplasmic extracts were incubated with anti-FLAG M2 affinity gel in binding buffer [150 mM NaCl, 3 mM $MgCl_2$, 10 mM tris-HCl (pH 7.4), and 0.25% NP-40] overnight at 4°C with rotation. Beads were then washed three to five times with ice-cold wash buffer [10 mM tris-HCl (pH 7.4), 1 mM EDTA, 150 mM NaCl, 0.35% Triton X-100, and 0.2 mM sodium orthovanadate]. Immunoprecipitates were eluted by heating in 2 × SDS loading buffer at 70°C for 10 min.

For TAF7 IP, the cytoplasmic extracts were incubated with 5 μg of TAF7 antibody or the control mouse IgG overnight at 4°C with gentle mixing, followed by addition of 50 μl of Pierce Protein G agarose (Thermo Fisher Scientific). The mixture was incubated for 2 hours at 4°C with gentle mixing, followed by three to five washes with IP buffer [25 mM tris-HCl (pH 7.4) and 150 mM NaCl]. IP products were then resuspended in 2 × SDS loading buffer and heated at 70°C for 10 min for elution.

For immunoblotting, proteins were separated on 12% SDS–polyacrylamide gel electrophoresis (SDS-PAGE) and transferred onto a nitrocellulose membrane (GE Healthcare). After blocking with 5% fat-free milk in TBST [10 mM tris-HCl (pH 8.0), 150 mM NaCl, and 0.05% Tween 20], the blots were incubated with the primary antibodies. The secondary antibodies IRDye800CM or IRDye680RD (LI-COR Biosciences) were used for protein detection.

Quantitation of the distribution of TAF7 between nucleus and cytoplasm was based on the intensity of antibody staining of TAF7 as determined by densitometry, corrected for the amounts of TBP in the cytoplasm and tubulin in the nucleus with the following equation: Nuclear TAF7 = amount of nuclear TAF7 (total cellular TBP/nuclear TBP) − amount of cytoplasmic TAF7 (nuclear tubulin/total cellular tubulin). Cytoplasmic TAF7 = total cellular TAF7 − nuclear TAF7.

In vitro protein pull-down assays

For in vitro pull-down, 500 ng of recombinant FLAG-tagged TAF7 proteins was incubated with 500 ng of recombinant human RPL8 protein (ab123188, Abcam) or 500 ng of recombinant human RPL5 protein (ab183222, Abcam) in binding buffer [150 mM NaCl, 3 mM $MgCl_2$, 10 mM tris-HCl (pH 7.4), and 0.25% NP-40] for 2 hours at 4°C with rotation. The protein complex was pulled down with anti-FLAG M2 affinity gel for 2 hours at 4°C with rotation. Proteins were eluted from the beads in 2 × SDS loading buffer.

Immunofluorescence and PLA

Immunofluorescence staining was performed as previously described (*40*). Briefly, MEF, HeLa, or HeLa S3 cells were fixed with 4% paraformaldehyde for 15 min, permeabilized with 0.5% Triton X-100, and blocked with 5% goat serum and 1% BSA for 1 hour at room temperature. Cells were then incubated with primary antibodies overnight at 4°C followed by incubation with goat anti-mouse IgG (H + L) highly cross-adsorbed secondary antibody, Alexa Fluor 568 (1:500 dilution, Invitrogen) for 1 hour at room temperature. The stained cells were mounted on slides in ProLong Gold Antifade Mountant with 4′,6-diamidino-2-phenylindole (DAPI). Cells were visualized with a Zeiss LSM880 Multi-photon Microscope (Zeiss). For the 5-Fu incorporation assay, MEF or HeLa S3 cells were incubated in DMEM containing 200 mM 5-Fu for 10 min at 37°C before immunostaining with anti-BrdU antibody (1:400 dilution, B2531, MilliporeSigma).

PLA was conducted in HeLa cells using the Duolink In Situ Red Starter Kit Mouse/Rabbit (DUO92101, MilliporeSigma) according to the manufacturer's protocol (MilliporeSigma). The antibodies used in PLA are as follows: anti-TAF7 (1:400 dilution), anti-TBP (1:400 dilution), anti-RPL5 (1:600 dilution), anti-RPL8 (1:600 dilution), anti-XPO1 (1:800 dilution), anti-eIF5B (1:400 dilution), and anti-hnRNP U (1:400 dilution).

In vitro RNA binding assay

Recombinant FLAG-tagged TAF7 protein (10 μg) was incubated with 10 μg of total RNA of HeLa S3 cells at 4°C for 4 hours. TAF7-RNA complexes were isolated by IP using anti-FLAG M2 affinity gel. RNAs were released from the TAF7-RNA complexes by an acid phenol:chloroform (pH 4.5, Ambion) extraction. The RNAs were labeled at the 3′ end with cordycepin 5′-triphosphate [α-^{32}P] (PerkinElmer) by poly(A) polymerase (yeast) at 37°C for 20 min. The labeled RNAs were isolated with acid phenol:chloroform (pH 4.5) and examined in 8% sequencing gel.

RNA immunoprecipitation

RIP assays were performed as previously described (*41*) with cytoplasmic extracts. In brief, the cytoplasmic extracts from HeLa TAF7 (WT) cells were incubated with a suspension of Protein A–Sepharose (Sigma-Aldrich) that was precoated with 20 μg of either anti-TAF7 antibody or mouse IgG for 2 hours at 4°C. After washing in NT2 buffer [50 mM tris-HCl (pH 7.4), 150 mM NaCl, 1 mM $MgCl_2$, and 0.05% NP-40], RNAs were released from the TAF7-RNA complexes by proteinase K treatment followed by an acid phenol:chloroform (pH 4.5) extraction. RNA-seq was performed at the Next Generation Sequencing Facility, Center for Cancer Research at the National Cancer Institute, National Institutes of Health. cDNA libraries were prepared using the SMARTer Ultra Low RNA Kit for Illumina Sequencing and Illumina Nextera XT DNA Library Preparation Kit. The samples were sequenced as paired-end reads on the Illumina HiSeq4000.

Photoactivatable ribonucleoside–enhanced cross-linking and immunoprecipitation

PAR-CLIP was carried out as described using the cytoplasmic lysate from about 2×10^8 HeLa S3 TAF7 cells (*17*, *18*). Briefly, HeLa TAF7 (WT) cells were incubated with 100 μM 4SU in culture medium for 16 hours, followed by UV cross-linking at 312 nm. The cross-linked cells were then subjected to fractionation (described above) to isolate nuclear extracts and cytoplasmic extracts. TAF7-RNA complexes in cytoplasmic extracts were immunoprecipitated using anti-FLAG M2 affinity gel and treated with RNase T1. After SDS-PAGE separation of the TAF7-RNA complexes, the RNA fragments were released by protease K digestion and were further isolated using acid phenol:chloroform (pH 4.5). The recovered RNA was turned into cDNA libraries and sequenced. After basic analysis, the resulting sequence reads were mapped to the human genome (hg19).

Electrophoretic mobility shift assay

Recombinant HIV-1 Tat protein was purchased from Abcam (ab83353). Recombinant TAF7 protein was prepared as described above. TAR RNA (5′ GGCAGAUCUGAGCCU GGGAGCUCUCUGCC-3′) (*42*) and TARmut RNA (5′ GGCAGAAAGGAGCAUUGG AGCUCUCUGCC 3′) (*43*) were purchased from Dharmacon (Horizon Discovery). TAR duplexes were prepared by heating the RNA fragments (100 μM in diethyl pyrocarbonate–treated water) to 95°C for 5 min followed by quick cooling on ice for 10 min. Each EMSA reaction (20 μl) contained 20 pmol of RNA fragments, 5 to 20 pmol of TAF7 protein (or 50 to 100 pmol Tat protein), and binding buffer [30 mM tris-HCl (pH 8.0), 70 mM KCl, 5.5 mM $MgCl_2$, 0.01% NP-40, 1 mM dithiothreitol, and 12% glycerol]. The reactions were incubated at 25°C for 30 min and then subjected to 8% native PAGE at 200 V in 1 × tris-borate-EDTA buffer. The binding of TAF7 to TAR RNA was detected using the EMSA Kit (Invitrogen) according to the manufacturer's instructions.

Fast protein liquid chromatography

Cytoplasmic extracts (contain about 5 mg of proteins) from HeLa cells or from TMD8 B lymphoma cells were diluted into 1 ml with BC100 buffer [20 mM tris-HCl (pH 7.4), 100 mM KCl, 10% glycerol, and 0.2 mM EDTA] and applied to a Superose 6 10/300 GL (GE Healthcare) column in ÄKTA FPLC system (GE Healthcare) according to the manufacturer's instructions. The column was equilibrated with BC100 buffer and eluted with the same buffer at 0.3 ml/min. The eluent was monitored at 280 nm and collected in 1-ml fractions. Chromatographic fractions were analyzed by SDS-PAGE followed by immunoblotting. The molecular weight of TAF7 complex was determined according to the standard curve of Gel Filtration Markers (MWGF1000, MilliporeSigma).

Polysome profiling

Polysome profiling was performed as described by Gandin *et al.* (*44*). Briefly, cells were incubated with cycloheximide (CHX, 100 μg/ml) in medium for 5 min at 37°C before harvesting. The cytoplasmic extracts (the equivalent of 10 A260 units) were layered onto 12 ml of 10 to 50% sucrose gradient prepared in sucrose gradient buffer [20 mM Hepes (pH 7.6), 100 mM KCl, 5 mM $MgCl_2$, CHX (10 μg/ml), protease inhibitor cocktail, and RNase inhibitor (100 U/ml)] and centrifuged at 36,000 rpm for 2.5 hours at 4°C using SW41Ti rotor (Beckman). Gradients were fractionated, and the absorbance at 254 nm was monitored. Collected fractions were analyzed by immunoblotting.

siRNA transfection

For TAF7 siRNA transient transfections, 50 nM of the TAF7 (NES) siRNA sense (5′ GCAGCAGUGAGGAUGAAGAUU 3′), TAF7 (NES) siRNA antisense (5′-P UCUUCAUCCUCACUGCUGCUU 3′), or the TAF7 (RBD) siRNA sense (5′ CUAAAGAAUGUCAGGAAGAUU 3′), TAF7 (RBD) siRNA antisense (5′ UCUUCCUGACAUUCUUUAGUU 3′), or the ON-TARGETplus Nontargeting Control Pool (D-001810-10-05, Dharmacon) were transfected into HeLa S3 cells using Dharma FECT4 Transfection Reagent according to the manufacturer's protocol. Cells were harvested 48 hours after transfection, and total cell extracts were analyzed for TAF7 protein levels by anti-TAF7 immunoblotting.

SUnSET assay

The SUnSET assay was used to monitor protein synthesis (*21*). In brief, HeLa S3 cells or MEF cells were incubated with puromycin (10 μg/ml) in DMEM medium for 15 min at 37°C. After washing twice with the medium, the cells were incubated in medium for 45 min at 37°C. For SUnSET-FACS, cells were harvested and stained for puromycin using 0.5 μg of Alexa Fluor 647–conjugated anti-puromycin (12D10) monoclonal antibody (MABE343-AF647, Millipore). Intracellular staining was performed using the Fixation/Permeabilization Solution Kit (BD Biosciences) according to the manufacturer's protocol. After staining, cells were immediately subjected to FACS analysis using a BD LSRFortessa flow cytometer.

Real-time PCR

Relative transcript levels and transcript distribution between the nucleus and the cytoplasm of Haspin, SMARCC2, DPP9, and luciferase were evaluated by real-time PCR. For relative transcript levels, total RNA was isolated from MEF TAF7 (WT) + Cre and TAF7 (ΔNES) + Cre cells. For transcript distribution, RNA was isolated from the nuclear extracts and the cytoplasmic extracts of MEF TAF7 (WT/NLS) + Cre and MEF TAF7 (RBD/NLS) + Cre cells or from the nuclear and the cytoplasmic extracts of HeLa TAF7 (WT/NLS) + siRNA and HeLa TAF7 (RBD/NLS) + siRNA cells. RNA extraction was performed using RNeasy Plus Mini Kit (Qiagen), followed by treatment with RNase free-DNase (Qiagen). Reverse transcription reaction was performed using Superscript III First-Strand Synthesis System (Invitrogen) and random primers. The resultant cDNA was subjected to real-time PCR analysis in QuantStudioTM 6 Flex Real-Time PCR System (Applied Biosystems) using SYBR Green PCR Master Mix (Applied Biosystems). For relative transcript levels, 18S rRNA was used as an internal control to normalize mRNA abundance, and the comparative Ct (ΔΔCt) method was used to quantify the relative levels of gene expression. For transcript distribution between the nucleus and cytoplasm, glyceraldehyde-3-phosphate dehydrogenase (F: 5′ TGTGTCCGTCGTGGATCTGA 3′; R: 5′ CCTGCTTCACCACCTTCTTGA 3′) was used as an internal control to normalize mRNA abundance, and the standard curve method was used to quantify the levels of gene expression. Three biological replicates with three PCR replicates each were performed. Gene-specific primers used for real-time PCR are as follows: Haspin F: 5′ GAGTCGACCAGAGAGACTATGA 3′, Haspin R: 5′ CCGTTGCTTCTTGCTGTTTC 3′; SMARCC2 F: 5′ GCGCTATCATGAGGGTCCAT 3′, SMARCC2 R: 5′ CTTCGGCTGAAGAGGAACCA 3′; DPP9 F: 5′ ATGGAGCGTCGCGTGTGAG 3′, DPP9 R: 5′ AAAGGGTCCAAGGAGCTTCCA 3′; and luciferase F: 5′ CCAGGTATCAGGCAAGGATATG 3′, luciferase R: 5′ GTTCGTCTTCGTCCCAGTAAG 3′.

Data analysis

RNA-seq and RIP-seq reads were aligned to human reference genome (hg19) using STAR aligner with the default parameters (*45*). Raw read counts were obtained using htseq-count (*46*) and normalized for further analysis using the built-in normalization algorithms of DESeq2 (*47*). All differential expression analysis was performed with DESeq2, and a gene was considered as differentially expressed between two groups when its fold change >2 and false discovery rate adjusted P value < 0.01. Statistical testing and downstream analyses were performed in R.

PAR-CLIP data were analyzed using PARalyzer (*48*) with default parameters. Replicated experiments were pooled for the downstream analysis. Metagene analysis of PAR-CLIP T-to-C conversion site distribution was performed using R package Guitar (*49*). Sequence-structure RNA binding motifs were predicted using ssHMM (*19*).

Statistical analysis

All of the experiments reported here have been performed at least twice, most of them three times, as biological replicates each with means ± SD of at least three independent experiments. The P values indicate statistical significance, which is obtained using Student's t test (two-tailed, unpaired).

SUPPLEMENTARY MATERIALS

Supplementary material for this article is available at https://science.org/doi/10.1126/sciadv.abi5751

View/request a protocol for this paper from *Bio-protocol*.

REFERENCES AND NOTES

1. M. Choder, Rpb4 and Rpb7: Subunits of RNA polymerase II and beyond. *Trends Biochem. Sci.* **29**, 674–681 (2004).
2. L. Harel-Sharvit, N. Eldad, G. Haimovich, O. Barkai, L. Duek, M. Choder, RNA polymerase II subunits link transcription and mRNA decay to translation. *Cell* **143**, 552–563 (2010).
3. S. Paz, A. Ritchie, C. Mauer, M. Caputi, The RNA binding protein SRSF1 is a master switch of gene expression and regulation in the immune system. *Cytokine Growth Factor Rev.* **57**, 19–26 (2021).
4. V. Marcel, F. Catez, J. J. Diaz, p53, a translational regulator: Contribution to its tumour-suppressor activity. *Oncogene* **34**, 5513–5523 (2015).
5. A. Gegonne, J. D. Weissman, D. S. Singer, TAFII55 binding to TAFII250 inhibits its acetyltransferase activity. *Proc. Natl. Acad. Sci. U.S.A.* **98**, 12432–12437 (2001).
6. C. A. Mizzen, X. J. Yang, T. Kokubo, J. E. Brownell, A. J. Bannister, T. Owen-Hughes, J. Workman, L. Wang, S. L. Berger, T. Kouzarides, Y. Nakatani, C. D. Allis, The TAF(II)250 subunit of TFIID has histone acetyltransferase activity. *Cell* **87**, 1261–1270 (1996).
7. J. D. Weissman, J. A. Brown, T. K. Howcroft, J. Hwang, A. Chawla, P. A. Roche, L. Schiltz, Y. Nakatani, D. S. Singer, HIV-1 tat binds TAFII250 and represses TAFII250-dependent transcription of major histocompatibility class I genes. *Proc. Natl. Acad. Sci. U.S.A.* **95**, 11601–11606 (1998).
8. A. Gegonne, J. D. Weissman, M. Zhou, J. N. Brady, D. S. Singer, TAF7: A possible transcription initiation check-point regulator. *Proc. Natl. Acad. Sci. U.S.A.* **103**, 602–607 (2006).
9. A. Gegonne, J. D. Weissman, H. Lu, M. Zhou, A. Dasgupta, R. Ribble, J. N. Brady, D. S. Singer, TFIID component TAF7 functionally interacts with both TFIIH and P-TEFb. *Proc. Natl. Acad. Sci. U.S.A.* **105**, 5367–5372 (2008).
10. B. N. Devaiah, D. S. Singer, Cross-talk among RNA polymerase II kinases modulates C-terminal domain phosphorylation. *J. Biol. Chem.* **287**, 38755–38766 (2012).
11. A. Gegonne, B. N. Devaiah, D. S. Singer, TAF7: Traffic controller in transcription initiation. *Transcription* **4**, 29–33 (2013).
12. B. N. Devaiah, H. Lu, A. Gegonne, Z. Sercan, H. Zhang, R. J. Clifford, M. P. Lee, D. S. Singer, Novel functions for TAF7, a regulator of TAF1-independent transcription. *J. Biol. Chem.* **285**, 38772–38780 (2010).
13. A. Gegonne, X. Tai, J. Zhang, G. Wu, J. Zhu, A. Yoshimoto, J. Hanson, C. Cultraro, Q. R. Chen, T. Guinter, Z. Yang, K. Hathcock, A. Singer, J. Rodriguez-Canales, L. Tessarollo, S. Mackem, D. Meerzaman, K. Buetow, D. S. Singer, The general transcription factor TAF7 is essential for embryonic development but not essential for the survival or differentiation of mature T cells. *Mol. Cell. Biol.* **32**, 1984–1997 (2012).
14. J. C. Dantonel, K. G. Murthy, J. L. Manley, L. Tora, Transcription factor TFIID recruits factor CPSF for formation of 3′ end of mRNA. *Nature* **389**, 399–402 (1997).
15. T. Shibuya, S. Tsuneyoshi, A. K. Azad, S. Urushiyama, Y. Ohshima, T. Tani, Characterization of the ptr6(+) gene in fission yeast: A possible involvement of a transcriptional coactivator TAF in nucleocytoplasmic transport of mRNA. *Genetics* **152**, 869–880 (1999).
16. N. C. Bauer, P. W. Doetsch, A. H. Corbett, Mechanisms regulating protein localization. *Traffic* **16**, 1039–1061 (2015).
17. M. Hafner, M. Landthaler, L. Burger, M. Khorshid, J. Hausser, P. Berninger, A. Rothballer, M. Ascano, A. C. Jungkamp, M. Munschauer, A. Ulrich, G. S. Wardle, S. Dewell, M. Zavolan, T. Tuschl, PAR-CliP—A method to identify transcriptome-wide the binding sites of RNA binding proteins. *J. Vis. Exp.* 2034 (2010).
18. D. Benhalevy, H. L. McFarland, A. A. Sarshad, M. Hafner, PAR-CLIP and streamlined small RNA cDNA library preparation protocol for the identification of RNA binding protein target sites. *Methods* **118-119**, 41–49 (2017).
19. D. Heller, R. Krestel, U. Ohler, M. Vingron, A. Marsico, ssHMM: Extracting intuitive sequence-structure motifs from high-throughput RNA-binding protein data. *Nucleic Acids Res.* **45**, 11004–11018 (2017).
20. A. R. Gruber, R. Lorenz, S. H. Bernhart, R. Neuboock, I. L. Hofacker, The Vienna RNA websuite. *Nucleic Acids Res.* **36**, W70–W74 (2008).
21. E. K. Schmidt, G. Clavarino, M. Ceppi, P. Pierre, SUnSET, a nonradioactive method to monitor protein synthesis. *Nat. Methods* **6**, 275–277 (2009).
22. C. Dingwall, I. Ernberg, M. J. Gait, S. M. Green, S. Heaphy, J. Karn, A. D. Lowe, M. Singh, M. A. Skinner, R. Valerio, Human immunodeficiency virus 1 tat protein binds trans-activation-responsive region (TAR) RNA in vitro. *Proc. Natl. Acad. Sci. U.S.A.* **86**, 6925–6929 (1989).
23. J. Karn, C. Dingwall, J. T. Finch, S. Heaphy, M. J. Gait, RNA binding by the tat and rev proteins of HIV-1. *Biochimie* **73**, 9–16 (1991).
24. M. C. Lai, S. W. Wang, L. Cheng, W. Y. Tarn, S. J. Tsai, H. S. Sun, Human DDX3 interacts with the HIV-1 Tat protein to facilitate viral mRNA translation. *PLOS ONE* **8**, e68665 (2013).
25. R. D. Bouwman, A. Palser, C. M. Parry, E. Coulter, J. Rasaiyaah, P. Kellam, R. G. Jenner, Human immunodeficiency virus Tat associates with a specific set of cellular RNAs. *Retrovirology* **11**, 53 (2014).
26. M. Kuciak, C. Gabus, R. Ivanyi-Nagy, K. Semrad, R. Storchak, O. Chaloin, S. Muller, Y. Mély, J. L. Darlix, The HIV-1 transcriptional activator Tat has potent nucleic acid chaperoning activities in vitro. *Nucleic Acids Res.* **36**, 3389–3400 (2008).
27. K. M. Weeks, C. Ampe, S. C. Schultz, T. A. Steitz, D. M. Crothers, Fragments of the Hiv-1 tat protein specifically bind Tar Rna. *Science* **249**, 1281–1285 (1990).
28. A. D. Frankel, Peptide models of the Tat-TAR Protein-RNA interaction. *Protein Sci.* **1**, 1539–1542 (1992).
29. M. S. Zhou, M. A. Halanski, M. F. Radonovich, F. Kashanchi, J. Peng, D. H. Price, J. N. Brady, Tat modifies the activity of CDK9 to phosphorylate serine 5 of the RNA polymerase II carboxyl-terminal domain during human immunodeficiency virus type 1 transcription. *Mol. Cell. Biol.* **20**, 5077–5086 (2000).
30. T. P. Cujec, H. Okamoto, K. Fujinaga, J. Meyer, H. Chamberlin, D. O. Morgan, B. M. Peterlin, The HIV transactivator TAT binds to the CDK-activating kinase and activates the phosphorylation of the carboxy-terminal domain of RNA polymerase II. *Genes Dev.* **11**, 2645–2657 (1997).
31. N. Charnay, R. Ivanyi-Nagy, R. Soto-Rifo, T. Ohlmann, M. López-Lastra, J. L. Darlix, Mechanism of HIV-1 Tat RNA translation and its activation by the Tat protein. *Retrovirology* **6**, 74 (2009).
32. D. N. SenGupta, B. Berkhout, A. Gatignol, A. M. Zhou, R. H. Silverman, Direct evidence for translational regulation by leader RNA and Tat protein of human immunodeficiency virus type 1. *Proc. Natl. Acad. Sci. U.S.A.* **87**, 7492–7496 (1990).
33. S. Hutten, R. H. Kehlenbach, CRM1-mediated nuclear export: To the pore and beyond. *Trends Cell Biol.* **17**, 193–201 (2007).
34. A. Kohler, E. Hurt, Exporting RNA from the nucleus to the cytoplasm. *Nat. Rev. Mol. Cell Biol.* **8**, 761–773 (2007).
35. U. Fischer, S. Meyer, M. Teufel, C. Heckel, R. Lührmann, G. Rautmann, Evidence that HIV-1 Rev directly promotes the nuclear export of unspliced RNA. *EMBO J.* **13**, 4105–4112 (1994).
36. S. Pinol-Roma, G. Dreyfuss, Shuttling of pre-mRNA binding proteins between nucleus and cytoplasm. *Nature* **355**, 730–732 (1992).
37. C. S. Hill, Nucleocytoplasmic shuttling of Smad proteins. *Cell Res.* **19**, 36–46 (2009).
38. T. Meyer, U. Vinkemeier, Nucleocytoplasmic shuttling of STAT transcription factors. *Eur. J. Biochem.* **271**, 4606–4612 (2004).
39. H. Takahashi, I. Takigawa, M. Watanabe, D. Anwar, M. Shibata, C. Tomomori-Sato, S. Sato, A. Ranjan, C. W. Seidel, T. Tsukiyama, W. Mizushima, M. Hayashi, Y. Ohkawa, J. W. Conaway, R. C. Conaway, S. Hatakeyama, MED26 regulates the transcription of snRNA genes through the recruitment of little elongation complex. *Nat. Commun.* **6**, 5941 (2015).
40. B. N. Devaiah, C. Case-Borden, A. Gegonne, C. H. Hsu, Q. Chen, D. Meerzaman, A. Dey, K. Ozato, D. S. Singer, BRD4 is a histone acetyltransferase that evicts nucleosomes from chromatin. *Nat. Struct. Mol. Biol.* **23**, 540–548 (2016).
41. J. D. Keene, J. M. Komisarow, M. B. Friedersdorf, RIP-Chip: The isolation and identification of mRNAs, microRNAs and protein components of ribonucleoprotein complexes from cell extracts. *Nat. Protoc.* **1**, 302–307 (2006).

42. S. Kumar, P. Kellish, W. E. Robinson Jr., D. Wang, D. H. Appella, D. P. Arya, Click dimers to target HIV TAR RNA conformation. *Biochemistry* **51**, 2331–2347 (2012).
43. N. Mueller, A. O. Pasternak, B. Klaver, M. Cornelissen, B. Berkhout, A. T. Das, The HIV-1 Tat protein enhances splicing at the major splice donor site. *J. Virol.* **92**, e01855-17 (2018).
44. V. Gandin, K. Sikström, T. Alain, M. Morita, S. McLaughlan, O. Larsson, I. Topisirovic, Polysome fractionation and analysis of mammalian translatomes on a genome-wide scale. *J. Vis. Exp.* 51455 (2014).
45. A. Dobin, C. A. Davis, F. Schlesinger, J. Drenkow, C. Zaleski, S. Jha, P. Batut, M. Chaisson, T. R. Gingeras, STAR: Ultrafast universal RNA-seq aligner. *Bioinformatics* **29**, 15–21 (2013).
46. S. Anders, P. T. Pyl, W. Huber, HTSeq—A Python framework to work with high-throughput sequencing data. *Bioinformatics* **31**, 166–169 (2015).
47. M. I. Love, W. Huber, S. Anders, Moderated estimation of fold change and dispersion for RNA-seq data with DESeq2. *Genome Biol.* **15**, 550 (2014).
48. D. L. Corcoran, S. Georgiev, N. Mukherjee, E. Gottwein, R. L. Skalsky, J. D. Keene, U. Ohler, PARalyzer: Definition of RNA binding sites from PAR-CLIP short-read sequence data. *Genome Biol.* **12**, R79 (2011).
49. X. Cui, Z. Wei, L. Zhang, H. Liu, L. Sun, S. W. Zhang, Y. Huang, J. Meng, Guitar: An R/Bioconductor package for gene annotation guided transcriptomic analysis of RNA-related genomic features. *Biomed. Res. Int.* **2016**, 8367534 (2016).

Acknowledgments: We acknowledge D. Larson, T. Misteli, R. Sen, M. Palangat, and the members of the Singer laboratory for helpful discussions and critical reading of the manuscript. We also thank S. Sharrow, T. Adams, and A. Crossman for help with flow cytometry and J. Wisniewski for confocal microscopy. We thank the Lou Staudt laboratory for RMD8 B lymphoma cell extracts. **Funding:** This research was supported by the Intramural Research Program of Center for Cancer Research, National Cancer Institute, NIH. **Author contributions:** D.C. performed experiments, interpreted data, and wrote the manuscript; E.M., A.G., K.S., and B.A.L. performed experiments; Q.C. and D.M. performed bioinformatics analyses; X.W., M.H., and B.N.D. provided training and helped to design experiments; H.T. provided stably transfected cell lines; and D.S.S. designed experiments, interpreted data, and wrote the manuscript. **Competing interests:** The authors declare that they have no competing interests. **Data and materials availability:** All data needed to evaluate the conclusions in the paper are present in the paper and/or the Supplementary Materials. The high-throughput dataset generated during this study is available at GEO: GSE161671.

Submitted 20 March 2021
Accepted 22 October 2021
Published 10 December 2021
10.1126/sciadv.abi5751